ACS APPLIED MATERIALS & INTERFACES

www.acsami.org

Forum Article

In Operando, Photovoltaic, and Microscopic Evaluation of Recombination Centers in Halide Perovskite-Based Solar Cells

Arava Zohar, Michael Kulbak, Silver H. Turren-Cruz, Pabitra K. Nayak, Adi Kama, Anders Hagfeldt, Henry J Snaith, Gary Hodes,* and David Cahen*

Cite This: *ACS Appl. Mater. Interfaces* 2022, 14, 34171−34179

Read Online

ACCESS | Metrics & More | Article Recommendations | Supporting Information

ABSTRACT: The origin of the low densities of electrically active defects in Pb halide perovskite (HaP), a crucial factor for their use in photovoltaics, light emission, and radiation detection, remains a matter of discussion, in part because of the difficulty in determining these densities. Here, we present a powerful approach to assess the defect densities, based on electric field mapping in working HaP-based solar cells. The minority carrier diffusion lengths were deduced from the electric field profile, measured by electron beam-induced current (EBIC). The EBIC method was used earlier to get the first direct evidence for the n-i-p junction structure, at the heart of efficient HaP-based PV cells, and later by us and others for further HaP studies. This manuscript includes EBIC results on illuminated cell cross sections (in operando) at several light intensities to compare optoelectronic characteristics of different cells made by different groups in several laboratories. We then apply a simple, effective single-level defect model that allows deriving the densities (N_r) of the defect acting as recombination center. We find $N_r \approx 1 \times 10^{13}$ cm^{-3} for mixed A cation lead bromide-based HaP films and $\sim 1 \times 10^{14}$ cm^{-3} for $MAPbBr_3(Cl)$. As EBIC photocurrents are similar at the grain bulk and boundaries, we suggest that the defects are at the interfaces with selective contacts rather than in the HaP film. These results are relevant for photovoltaic devices as the EBIC responses distinguish clearly between high- and low-efficiency devices. The most efficient devices have n-i-p structures with a close-to-intrinsic HaP film, and the selective contacts then dictate the electric field strength throughout the HaP absorber.

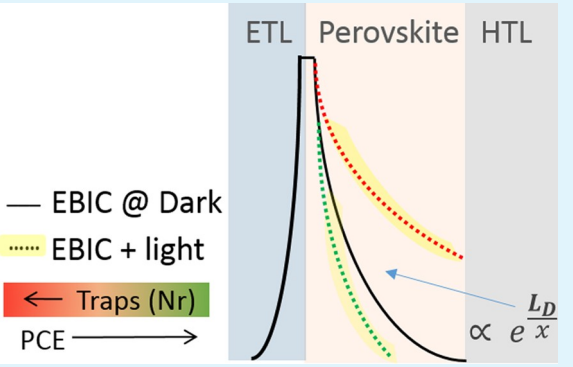

KEYWORDS: *defect states, diffusion length, p-i-n junction, Br-based perovskite, EBIC*

INTRODUCTION

Halide perovskites (HaPs), particularly those containing lead, have properties of high-quality semiconductor materials suitable for a solar cell application, especially because their preparation procedure requires low energy consumption (low temperatures, atmospheric pressure). The combination of sharp absorption onsets, low exciton binding energies, relatively long lifetimes of photogenerated carriers, and reasonable carrier mobilities reduces the energetic photovoltaic losses to yield high solar-to-electrical power conversion. Lead halide perovskite compounds, with mainly iodide as halide, have shown high conversion efficiencies (PCE ∼ 25%).[1] Higher bandgap HaPs, such as bromide-based ones, show lower power conversion (up to ∼10%), but they draw the attention of the community because of their higher open-circuit voltages (V_{OC} ∼ 1.6 V).[2] Those high voltages are required for applications in tandem solar cells, photoelectrochemical water splitting, and carbon dioxide (CO_2) reduction.[3,4]

We have argued that the crucial property that allows the phenomenal performance of lead HaP-based PV cells is the low defect density and/or the low optoelectronic activity of such defects.[5,6] Observables[7−9] that may reflect the density of optoelectronically active defects are carrier diffusion length and the sharpness of the optical absorption onset.[10] The main problem with the measurement of HaP electronic transport parameters is the extent to which method−model[11] combinations that are well-established for the common, tetrahedrally coordinated diamond structure-based semiconductors (e.g., SCLC, DLTS), remain valid here, which clearly impacts the reliability of the measurements.

Here we use an approach for in situ measurements of carrier diffusion lengths in HaPs, with and without illumination, to mimic as much as possible the functionality of the HaP in an operating solar cell and to learn about the charge transport properties under working conditions. The novelty of this work is

Special Issue: Novel Trends in Halide Perovskites for Optoelectronic Applications

Received: May 10, 2021
Accepted: August 17, 2021
Published: August 30, 2021

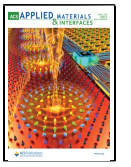

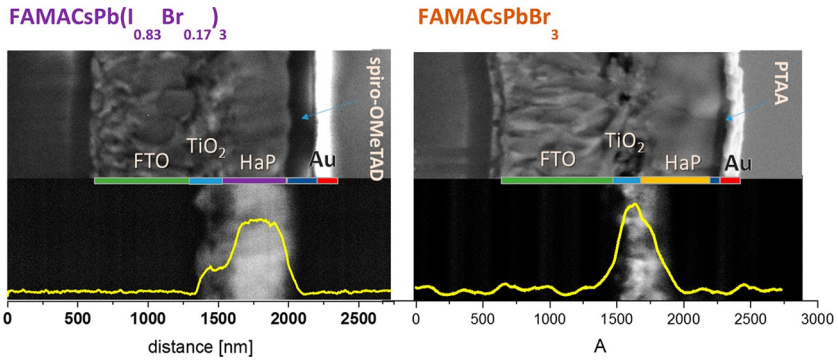

Figure 1. Secondary electron, SE, image (top) and EBIC image (bottom) of cross sections of solar cells made with bromide- and iodide-based perovskites. The EBIC profile line (yellow) is superimposed on the EBIC image. The solar device architecture is, from (left to right) FTO (green)/d-TiO_2 and mp-TiO_2 (light blue)/HaP/hole transport layer (dark blue)/Au (red). Left, (FAMACs)$Pb(I_{0.83}Br_{0.17})_3$ (purple); right, (FAMACs)$PbBr_3$ (orange).

that it allows a comparative evaluation of different HaP cells prepared by several different groups in different laboratories by looking at the electronic transport properties on a microscopic level. Those properties, including comparing effective electronically active defect concentrations, are most relevant for photovoltaic activity in working cells. Depending on the perovskite composition, the carrier length parameter that will dominate the EBIC decay, L_D, can be driven by the electric field or the carrier concentration gradient. As a result, L_D will be the drift (p-i-n) length for MAPI, or a combination of drift and diffusion (p-n), or the diffusion (p-n) length for $MAPbBr_3$. Therefore, we will extract L_D, the carrier diffusion/drift length, from the decay of the electron beam-induced current (EBIC) signal in the junction of the cell.[12,13] To learn more about the electronic behavior under working conditions, we use continuous background illumination, in addition to the local excitation by the electron beam, basing ourselves on earlier work, first on $CuInSe_2$[14] and more recently on HaPs.[15] A schematic of our setup is given in Figure S1, and a detailed explanation about the EBIC method and the estimated electric field at the junction for an operating cell can be found in part A of the Supporting Information.

The EBIC will now reflect the illumination-modified band positions, i.e., a situation close to that in an operating solar cell. The measured results suggest that the illumination effect is not a simple addition of photogenerated carriers to electron-beam-generated ones as expected from a superposition of the photo- and electrovoltaic processes. The often observed light-dark crossover in the $J-V$ curve indicates a nonlinear relationship between current and light intensity. It supports the hypothesis that defect states with energy levels within the bandgap are being occupied under illumination. Therefore, using EBIC under dark and illumination conditions, we can extract the mobility-lifetime product to predict an effective trap level energy and density that limits charge transport in the HaP materials.

RESULTS AND DISCUSSION

Electric Field Profile within a Solar Cell Device. Figure 1 presents SEM cross sections of (FA,MA,Cs)$Pb(I,Br)_3$ (left) and FA,MA,Cs)$PbBr_3$ (right) solar cells (top) with the corresponding EBIC images below them. The experimental details and the sample preparation can be found in part A in the Supporting Information. The left solar cell comprises an iodide-based perovskite layer between an electron transport layer, ETL (FTO/d-TiO_2 mp-TiO_2), and a hole transport layer, HTL (spiro-OMeTAD/Au), that serve as contacts. The right solar cell is a Br-based HaP sandwiched between FTO/d-TiO_2 mp-TiO_2 and PTAA (poly triarylamine)/Au. The secondary electron, SE, images facilitate correlation of the position from where current is generated by the e-beam in the cross sections, with the magnitude of current extracted, along the solar cell cross section. The acceleration voltage of the electrons used for the SE images is 2 keV, and the measured beam currents were 3−6 pA. For the experimental conditions used here, the generation volume, i.e., the region in which secondary electrons are generated because of primary beam electrons interacting with the semiconductor, is estimated to have an ∼20 nm diameter and down to a depth <100 nm (more details are given in the Supporting Information).

For the iodide-based HaP, the EBIC signal drops only at the interfaces with the selective contacts and shows an excellent spatial match to where the HaP layer is positioned in the cross section. The uniform EBIC signal throughout the iodide-based perovskite layer is consistent with previous results of ours,[16−18] and it supports our conclusion (see below) that iodide-based perovskite PVs have a n-i-p junction instead of a p-n one.

The Br-based perovskite has a similar ETL as the iodide one but a different HTL layer. The HTL contribution to the cell's built-in voltage was experimentally found to be minor (<100 mV).[19] Kedem et al. also showed that the back contact (evaporated metal) component would dictate the electric field as it inverts the HaP to become p-type material.[12] In this work, all the measured cells had Au as the metal back contact. The observed profile line of the Br-based cell EBIC shows a peak shape close to the TiO_2/HaP interface, followed by a monoexponential decay within the HaP layer toward the HaP/PTAA interface. This EBIC signal is different from the iodine perovskite-based cells, where the peak-like profile resembles a n-i-p junction. The signal decay represents a decrease of charge collection for the case where the photoabsorber layer width is larger than the minority diffusion length (electron diffusion length for a p-type material). This observation is consistent with the n-type behavior of TiO_2 and the p-type behavior of $MAPbBr_3$ that is inverted by the Au contact. The decay of the EBIC signal in a cell configuration[12,13] is proportional to the carrier diffusion/drift lengths (L_D). A scheme of the EBIC signals for p-n or n-i-n junctions with different L_D values is presented in Figure S3 and explained in part B in the Supporting Information.

https://doi.org/10.1021/acsami.1c08675
ACS Appl. Mater. Interfaces 2022, 14, 34171−34179

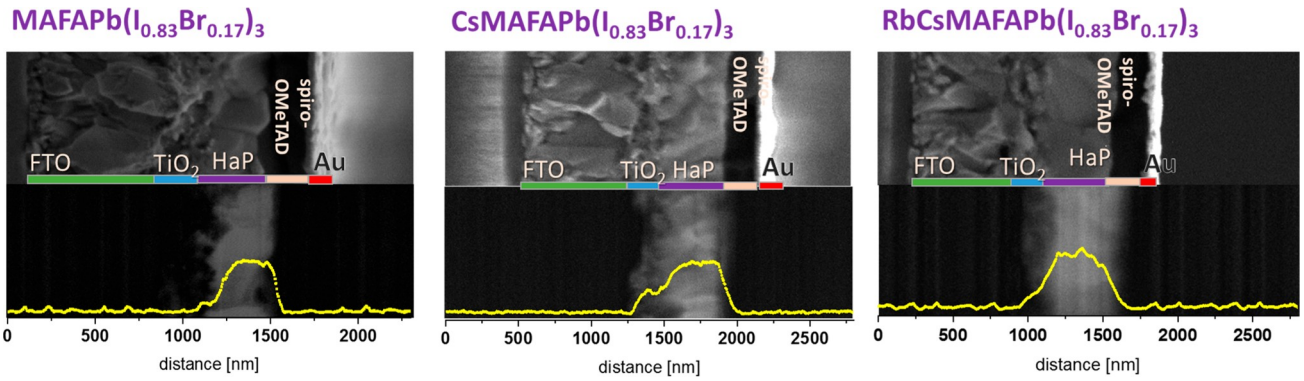

Figure 2. SE image (top) and corresponding EBIC image (bottom) of cross sections of PV devices made with iodide-based perovskites with different A cation combinations. The selective contacts are FTO (green)/d-TiO_2 and mp-TiO_2 (light blue)/(A cation)PbI_3 HaP (purple)/hole transport layer (cream)/Au (red). All the cells were fabricated at EPFL.[20]

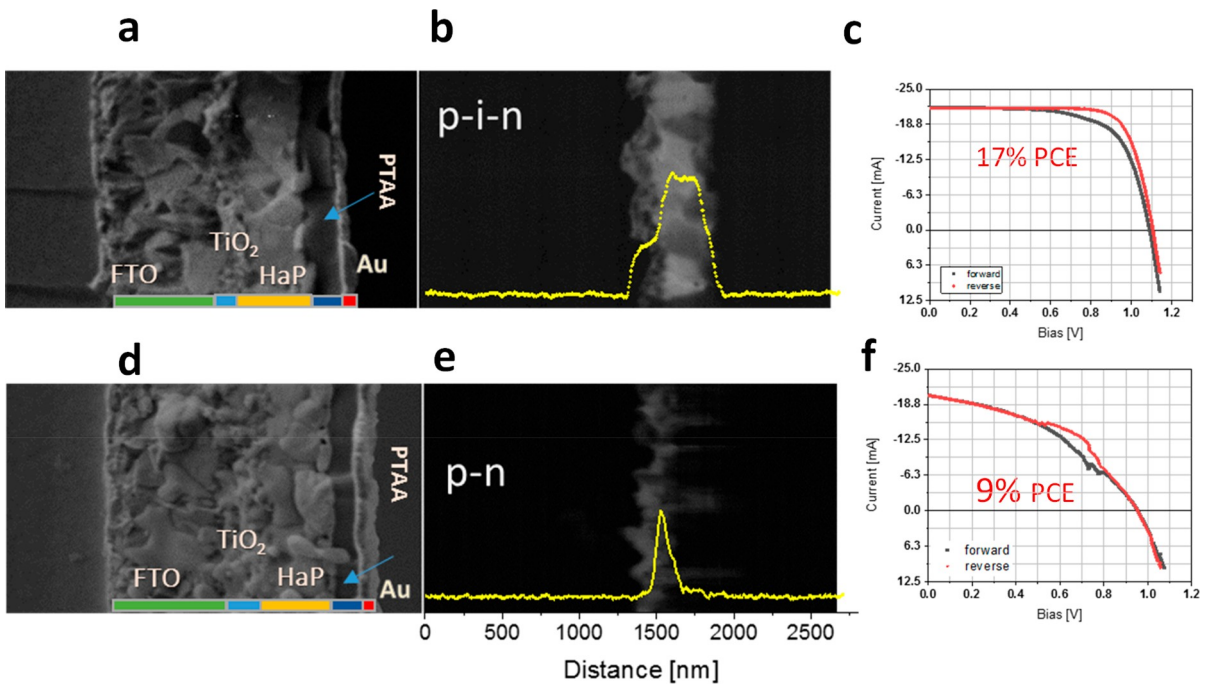

Figure 3. Comparison between SE and EBIC cross sections, and performance of two cells made from iodide-based perovskite of FTO/d-TiO_2/mp-TiO_2/FAMAPb($I_{0.83}Br_{0.17}$)$_3$/PTAA/Au cell. (a, d) SE images. (b, e) EBIC images. (c, f) *I*–*V* curves of the cells under illumination and their power conversion efficiencies.

As part of the efforts to achieve stability, reproducibility, and higher power conversion efficiency, many groups varied the A cation composition. Cell performance was often very dependent on the specific combinations of A cations for iodide-based perovskites. Here, we compare EBIC and SE images of different A cation compositions made by four different groups (from the Weizmann Institute[21], University of Oxford,[22] Bar-Ilan University, and EPFLausanne;[20] Figure S4 and sample preparation in part C in the Supporting Information) to learn about the effect of the A cation on the electric field in a cell and the impact of sample preparation in different laboratories. Figure 2 shows three samples made at EPFL for all-iodide-based perovskite solar devices. The cells show similar EBIC profiles, regardless of the A composition, consistent with the n-i-p junction structure that we find for all iodide-HaP-based junctions. For example, we showed previously that this structure also holds for $MAPbI_3$ and that it preserved its n-i-p shape also after beam damage that occurs because of multiple scans[17] (see Figure S5). Therefore, we conclude that, because of the small bandgap of iodide-based HaPs, the HaP layers are sufficiently intrinsic (and thin enough) that the entire HaP layer acts as a depleted layer in the junction. We find, furthermore, from our results, that the L_D values (drift for the MAPI case) are long (relative to the HaP layer thickness), resulting in a high current density collected from the MAPI solar device configuration. In addition. the EBIC measurement supports the idea that the A site does not significantly affect the density of electrically active defects in $APbI_3$ HaPs.

The electric field throughout the photoabsorber layer enhances charge separation and transport. Therefore, the maximum charge collection depends on whether the HaP material is intrinsic (or close to intrinsic) to form a n-i-p junction or not. For a n-i-p junction, the power conversion efficiency strongly depends on the strength of the electric field, which is governed by the selective contacts and not by the electrochemical potential (Fermi level) of the photoabsorber. We can

https://doi.org/10.1021/acsami.1c08675
ACS Appl. Mater. Interfaces 2022, 14, 34171−34179

test this by conducting a quality analysis for different cells produced by the same procedure but showing substantially different power conversion efficiencies (PCE). Figure 3 presents an example of two cells made with HaPs of identical composition (made from the same batch), one with a PCE of 17.4% (V_{oc} = 1.094 V, J_{sc} = −20.69 mA/cm^2, FF (fill factor) = 0.76, Figure 3c), and the second cell with a PCE of 9% (V_{oc} = 0.96 V, J_{sc} = 20.3 mA/cm^2, FF = 0.46 Figure 3f).

The V_{oc} and the J_{sc} of the two PV cells are not dramatically different, and only the FF shows different values. The fact that the V_{oc} of the two cells is similar suggests a similar built-in potential and supports the statement that the selective contacts dictate the electric field (the two cells have similar contacts). The J_{sc} data of the two cells show similar values, which represent the carrier collection between the electrodes in the absence of an applied potential. Under increasing forward bias, recombination will increase because of the decreasing built-in field. If the defect density within the gap is significant, the current (I) should drop rapidly compared to that expected from a classic diode behavior. Those defects may not significantly affect I_{SC} or the V_{OC} but will strongly affect the FF.

The SE images of both cells show a similar layered stack structure, emphasizing an equal HaP layer thickness and HaP grain size. However, the EBIC images are very different (Figure 3b, e). The higher-efficiency cell shows a uniform EBIC contrast (which we take here as representing the electrical field) across the HaP layer. The lower-efficiency cell shows an EBIC profile of a peak-like shape in the middle of the HaP layer, consistent with either a p−n junction or a low mobility-lifetime ($\mu\tau$) product. The first explanation (p−n junction) requires a moderate to high doping concentration (>1 × 10^{15} cm^{-3}); a low $\mu\tau$ is possible for materials with an L_D that is smaller than the film thickness (<200 nm) because $L_D = (\mu\tau)^{0.5}$. According to previous measurements done by Levine et al.,[23] I-based HaPs have L_D > 500 nm and τ > 200 ns for PCE = 9%. Therefore, higher doping is the likely explanation for the EBIC peak profile. Validation of this hypothesis was experimentally difficult as the atmosphere during the measurement, the preparation method, and the back contact of the HaP (including unintentional variations in these parameters) can affect the measured value of those materials because they tend to form as intrinsic semiconductors. Using the EBIC method, we can directly detect the electric field within the cell to provide information about the junction and estimate the doping concentration or the diffusion length of a bad or a good HaP cell. We emphasize that we assume the surface influence was the same for all samples because the exposure to the atmosphere between cross section preparation and insertion into the SEM chamber was minimal (see part A in the Supporting Information).

Grain Boundaries. It was commonly found that important parameters such as mobility, charge lifetimes, and thus, diffusion lengths and cell efficiencies improved with an increase in grain size (see ref 24), and this was interpreted as a contribution by grain boundaries (GBs) toward recombination for MAPI films.[21] It is furthermore noted in ref 25 that amorphous GBs were also found in $MAPbBr_3$ with increased PL and PL lifetimes compared to crystalline grain boundaries, and suggested this might explain the good performance of small-grained films. Edri et al., in the first reported EBIC study on HaP-based cells, found no change in EBIC contrast between the GBs and crystallite bulk in MAPI cells, suggesting that the GBs are benign in as far as recombination is concerned.[17,24] In their work (for different types of MAPI films), Kelvin probe force microscopy (KPFM) data are reported and showed a small potential difference between GBs and bulk (20 mV for MAPI(Cl))[24] and 40 mV for MAPI[17]); a barrier that small is not expected to affect PV performance around room temperature ($kT \approx 26$ meV), especially because illumination will reduce this barrier substantially.

Results of DFT-based calculations of the electronic band structure of MAPI show that native defects will form very shallow charge/discharge energy levels in the gap or even within the bands (resonances) and, therefore, will not be significant for recombination.[26] Although most such studies provide static pictures, a study of the Br vacancy point defect in $CsPbBr_3$ coupled DFT with molecular dynamics,[27] which showed large fluctuations of the (dis)charge level on sub-picosecond to tens of picosecond time scales, illustrating the problem of taking the static picture of defects literally for HaPs. Here we will use the concept of the defect and its associated defect level as a means to assess carrier recombination.

Sherkar et al.[28] claim that despite the presence of traps at GBs in the MAPI layer, trap-assisted recombination at interfaces is not the dominant recombination mechanism, at least in compact films, because the photogenerated charges neutralize the traps. Yun et al. even reported that the GBs in MAPI films on TiO_2 assist charge separation and collection, based on KPFM and conducting AFM current measurements under illumination,[29] which would result in a situation similar to what we discovered for CdTe and CIGS.[30,31] We note that except where noted otherwise, all the above studies were carried out on MAPI films and for other HaPs the situation may differ, especially for the more ionic all-inorganic ones.

We examined the charge recombination loss at the grain boundaries by measuring EBIC for a flat cross section of a cell. Normally, we use mechanical fracture to make cross section samples, which can often lead to nonflat surfaces because not everywhere will fracture occur along defined crystallographic cleavage planes. The resulting surface topography can cause charge accumulation or depletion on surfaces. Therefore, the EBIC signal can show a locally misleading electrical field profile. By using a gallium FIB to etch the surface, the EBIC signal is clean from topography artifacts due to leveling of the measured cross section. This treatment can provide direct information on whether the junction or the collected current are affected by the GBs. Figure 4 shows EBIC signals of an iodide-based perovskite solar cell as-cleaved (mechanically; see experimental details in

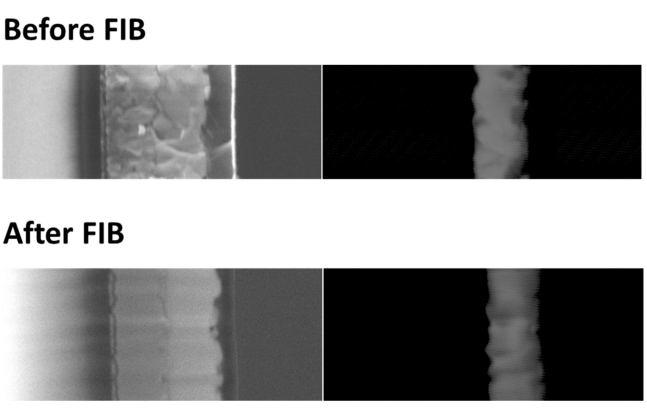

Figure 4. SEM (LEFT) and EBIC (RIGHT) images before and after FIB (Ga beam) treatment of FTO/TiO_2/HaP/spiro-OMeTAD/Au (samples from the Oxford group).

https://doi.org/10.1021/acsami.1c08675
ACS Appl. Mater. Interfaces 2022, 14, 34171−34179

the Supporting Information) and Ga-FIB polished samples. For both samples, the EBIC contrast across the HaP layer predominantly indicates a relatively uniform field and collection of both electrons and holes. Also, we do not see a current reduction at the grain boundaries in the fractured sample (where those are clearly visible in the SE image). From this, we conclude that grain boundaries do not reduce charge separation and transport or increase recombination in the HaP-based solar devices measured here. Furthermore, we can argue that surface passivation is not as crucial as for Si or GaAs because electrically, the HaP structure at the surface appears like that at the grain edges. This suggests that in these cells, the contacts of the HaP with the electron and hole transport layers do not introduce new defects with levels in the HaP bandgap. These results help to explain the tolerance of these solar cells to variations of grain size and morphology and are consistent with our early results, mentioned above, that showed only a few tens of millivolts voltage differences across grain boundaries.[17,24]

Defect Density. Defects in semiconductors can serve as recombination centers if their (dis)charge energy level is near midgap (similar hole and electron capture probabilities). Such deep levels enable so-called trap-assisted, i.e., SRH recombination, limiting open-circuit voltage (smaller quasi-Fermi level separation), charge mobilities, and carrier lifetimes. Well-established methods for in-gap state evaluation such as thermally stimulated current[32−34] and deep level transient spectroscopy[35,36] found that the density of states associated with the traps is up to about 1×10^{16} cm^{-3} for thin polycrystalline films of $MAPbI_2Br$ and $MAPbI_3$. Apart from the results obtained with these two methods, other groups suggested a few explanations of low defect density such as self-compensation, self-healing, lattice dynamic disorder, and ion migration[37−44] (relatively fast ion diffusion in HaP materials[40,45] can lead to screening of recombination centers). Those explanations are not contradictory and support the concept that ultrasensitive methods are needed to detect defect states in HaPs. Here, we use and argue in favor of a methodology that is not limited to film configuration and can reveal the actual trap density in a solar device under working conditions, viz., EBIC with additional background illumination. Free charge carriers are generated by local electron beam excitation and by the background light source that creates photogenerated carriers. The photogenerated carriers can modify the L_D, the square of the mobility−lifetime product. The EBIC image will visualize the electric field that is sensitive to changes in the density of generated carriers. By extracting the minority carrier diffusion length as a function of generation rate and applying it to the Rose model,[46] we can evaluate the defect densities. The results are not dependent on the origin of the defects, as we set the Rose model to account for one effective trap level (see below for more details). The generation rate is limited to the saturation value of the preamplifier that we use for the EBIC measurements 1 μA. Therefore, to reduce the light-induced photovoltaic current and detect only the electrovoltaic current, we used a beam-blanking system and a lock-in unit.

EBIC with and without background illumination on HaPs was measured by Kedem et al. for a $MAPbBr_3(Cl)$-based cell.[15] The electric field profile in the dark suggested an abrupt p−n junction, close to the $TiO_2/MAPbBr_3(Cl)$ interface, unlike the n-i-p type junctions with iodide HaPs. The larger bandgap of the bromide than that of the iodide HaP makes it harder to approach intrinsic doping densities needed for an HaP i region in a n-i-p junction. The diffusion length values, extracted from EBIC, fit with the observed properties of cells made with those materials, such as limited current density (1−4 mA/cm^2). The EBIC peak-shape became broader toward the HTL when background illumination was applied (Figure 5, which is adapted from Figure 4 in ref 15). The effect of background illumination on the EBIC signals was reversible, i.e., the EBIC profiles before and after the illumination were the same. By fitting the EBIC signal decay to a monoexponential function, effective values for the minority carrier diffusion length, L_D, were extracted (Figure S2). In this case, the electron diffusion length, L_D^e, increased by a factor of 2 with increasing illumination intensity. Such an increase in L_D^e is predicted by the Rose model for a generation rate (G) that yields equal hole and electron populations. This specific case occurs when the carriers, photogenerated by the additional light source (background illumination), eliminate (or neutralize) trap states above the Fermi level. For an effective one-trap level, we can calculate the effective defect density for $MAPbBr_3(Cl)$ based on the observed change of L_D^e in a given range of G (Figure S7).

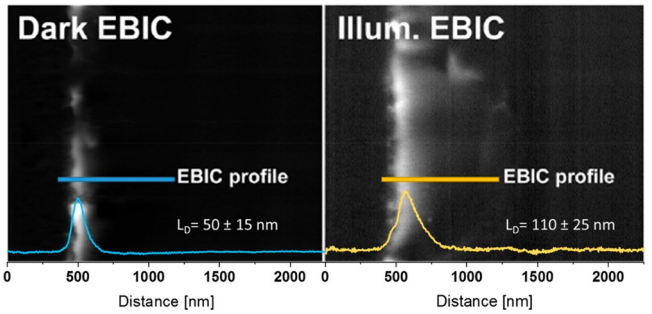

Figure 5. EBIC line scans, superimposed on EBIC images of a cross section of a solar cell composed of: $FTO/TiO_2/MAPbBr(Cl)_3/PTAA/Au$, with (right) and without (left) white light background illumination (which generated an ~20 nA photovoltaic current). The effective diffusion lengths were deduced from the EBIC line profiles by fitting to an exponential decay. The data are taken with permission from ref 8.

The Rose model predicts the L_D from the carrier populations in the bands and in the trap states. This model is described in detail by San et al.[46] and Levin et al.[23] for use with halide perovskites. The model is based on the charge neutrality principle, first-order rate equations, and for the HaPs of interest, the following assumptions:

(a) The material is a slightly p-type semiconductor.
(b) The photogenerated (n or p) carrier densities are much higher than those in the dark, i.e., $n, p \gg n_0, p_0$ where n_0 (p_0) is the electron (hole) concentration in the dark.
(c) Only e−h bimolecular and trap assistance recombination is assumed to occur. Auger recombination is neglected.
(d) At steady-state, the rate of generation and capture (or recombination) is the same for the two types of carriers

$$G = n/\tau_e = p/\tau_h \quad (1)$$

where G is the generation rate, in units of photons cm^{-3} s^{-1}, and τ is the lifetime of the corresponding charge carrier (s), which we can also be defined as

$$\tau_h = p/G \text{ and } \tau_e = n/G \quad (2)$$

The carrier diffusion lengths can be plotted as a function of the generation rate (G) using the Einstein relations:

$$L_D^e = \sqrt{\frac{kT\mu_e\tau_e}{q}} \text{ and } L_D^h = \sqrt{\frac{kT\mu_h\tau_h}{q}} \quad (3)$$

https://doi.org/10.1021/acsami.1c08675
ACS Appl. Mater. Interfaces 2022, 14, 34171−34179

where k is the Boltzmann constant, T is the temperature (in K), μ is the mobility, τ is the charge lifetime, and the e or h subscripts denote to which carrier the relevant property applies, electrons or holes.

The numerical solution of those equations using a *Matlab* code (see part D in the Supporting Information) is presented in Figure 6. The set of the equations was solved each time for a different total number of recombination centers

$$N_r(= p_r + n_r) \quad (4)$$

between 1×10^{13} and 1×10^{18} cm^{-3}. Each colored line represents the electron diffusion length, L_e (solid line), and the hole diffusion length L_D^h (dashed line) for a given N_r. The solid lines show three trends; a constant L_D, up to a specific G, then a small hill-like feature presents an increase followed by a decrease in the minority diffusion length. The peak position depends on the defect concentration (N_r), and it represents comparable hole and electron populations. The increase of L_D^e for higher G is a unique fingerprint that can help us to estimate the N_r. Note that N_r does not necessarily represent one level, but it is the density of the single level, assumed in the model, that represents the total effect of the densities of all the defect levels that are present in reality. The constants used here to solve the equations are the initial trapped minority carrier concentration $n_{r,0} = 1 \times 10^{12}$ [1/cm^3], the mobility, μ = 10 $cm^2/(V\ s)$, and the electrons, holes and the bimolecular recombination rates: $C_n = 1 \times 10^{-6}$ (cm^3/s), $C_p = 1 \times 10^{-8}$ (cm^3/s), $C_{bi} = 5 \times 10^{-10}$ (cm^3/s)[23] where we use the mobility value, reported by Motta et al.[47] The recombination coefficient will strongly influence the shape of the $L_D(G)$ curve and the extracted N_r values. Therefore, we took those values from Levine et al.[23] to yield a classic semiconduction behavior curve for a junction with a single trap level above the Fermi level under steady-state illumination. The extracted N_r values are estimated rather than precise numbers, but they do give a fair comparison between samples as the same model is used.

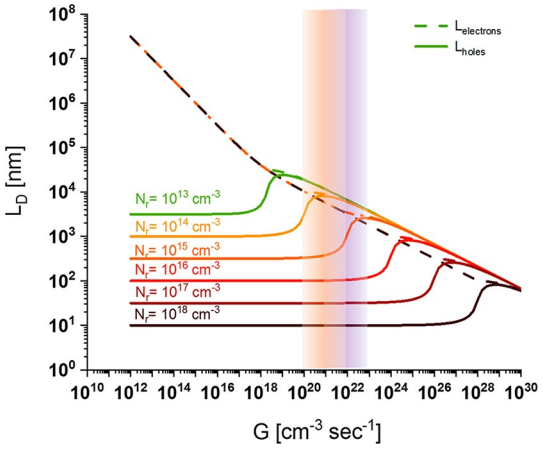

Figure 6. Diffusion lengths, L_D, of both charge carrier types, as a function of the photogeneration rate, G, as derived numerically, using the single effective trap state, by the Rose model[48] (see also SI) for $MAPbI_3$ and $MixAPbBr_3$ films. Each colored line (solid line for minority and dashed for majority charge carriers) is calculated for a given defect density. The majority charge carrier diffusion lengths (dashed lines) are hardly affected by the selected Nr values; therefore, all the dashed lines overlap. The generation rate (G) used for the MAPI was 10^{21}–10^{23} cm^{-3} sec^{-1} (vertical, left, orange stripe), and for the $MixAPbBr_3$ 10^{20}–10^{22} cm^{-3} sec^{-1} (vertical, right, purple stripe).

The generation rates, G, were calculated (see the Supporting Information) based on the HaP thickness and are highlighted in Figure 6. The L_D values extracted from the EBIC profiles (see Figure 5 and Figure S7) were fitted to the Rose model, which estimated $N_r \sim 1 \times 10^{14}$ cm^{-3} for $MAPbBr_3$(Cl). We will now use the combined EBIC profile data and the Rose model to evaluate MAPI and $MixAPbBr_3$ defect densities as well.

The EBIC signals for Mix(A cation)$PbBr_3$-based solar cells with and without illumination are presented in Figure 7 and Figure S6, where the linear dependence of L_D on the light intensity is shown as well. The EBIC profiles have a peak-like shape in the dark, and as the light intensity increased, the peak becomes narrower toward the ETL interface (Figure 7, right). The results show an EBIC profile trend for illumination intensities 2–12 mW/cm^2 (equal to $G = 1 \times 10^{20}$ to 1×10^{21} cm^{-3} s^{-1}) opposite to that found for the $MAPbBr_3$(Cl) cell (Figure 5). We note that the free carrier concentration, deduced earlier for the $MixAPbBr_3$ thin films, was 1×10^8 to 1×10^{10} cm^{-3}, at least 2 orders of magnitude lower than for $MAPbBr_3$(Cl) (1×10^{12} to 1×10^{14}).[21] The EBIC results fit the decrease in L_D for an increase in G derived from the Rose model at higher G values. A reduction of L_D can happen when the free carrier population is high enough to favor recombination. The estimated N_r values for MixAPbBr, based on those results, is $N_r < 1 \times 10^{13}$ cm^{-3}. Here, we measured only full cells containing a stack of materials. The HaP layer and each interface can contribute to the defect concentration. However, in the Br-based perovskites, the EBIC signal decay occurs only within the HaP. Therefore, the L_D used for the N_r calculation will be dominated by the HaP-related defects (within the layer and at the interface). This defect value can explain the higher performance measured for cells made with the mix cation-$PbBr_3$ perovskite than for those made with other A cation Br-based HaP films.

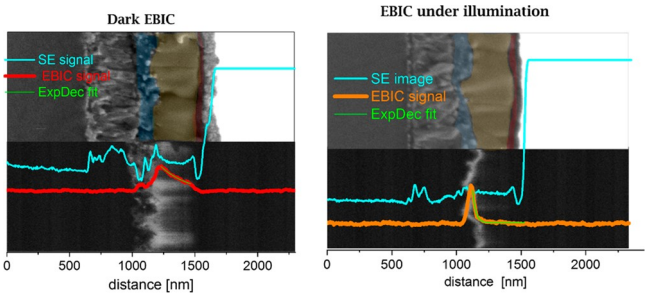

Figure 7. SE images of the cross section of a FTO/TiO_2/$MixAPbBr_3$/PTAA/Au solar cell: (A) dark and (B) with white light illumination.

Last, we show the effect of different illumination intensities on the EBIC signal from a MAPI solar cell cross section (Figure 8). The EBIC signal is uniform across the active layer, in the dark as well as with continuous white light intensity of 40–120 mW/cm^2 (equal to $G = 1 \times 10^{21}$ to 1×10^{22} generated carriers s^{-1} cm^{-3}). The EBIC intensity of the signal appears to be lower with background illumination. However, the absolute currents in the EBIC images with and without an additional light source are not comparable because the signal is modified by both the beam blanking and preamplifier (detection at different current ranges). The preamplifier current range was changed during the measurement to adjust the collected current increase as the generation rate increased. Therefore, we can only compare the profile line of the electric field and the width of the field. The

https://doi.org/10.1021/acsami.1c08675
ACS Appl. Mater. Interfaces 2022, 14, 34171–34179

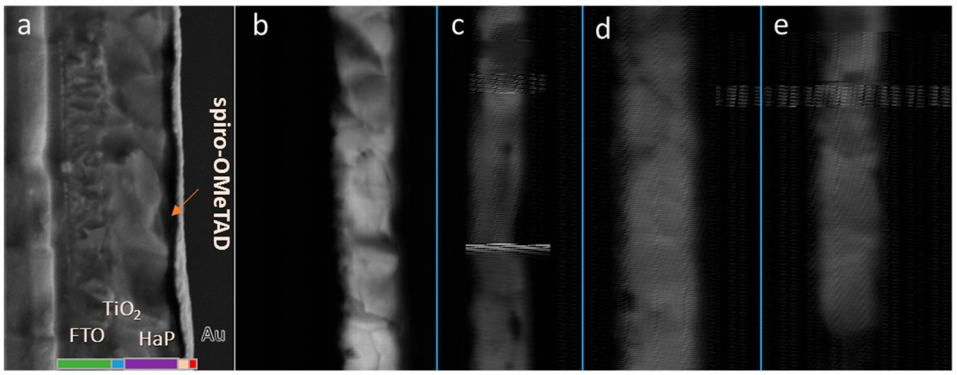

Figure 8. (a) SE image of the cross section of a MAPI-based cell. (b–e) EBIC images of that cross section (b) in the dark and (c–e) with increasing white background illumination intensity. The EBIC signals fit to the location of the HaP in the SE image of the cross section.

profiles of the EBIC signal in all cases show similar widths that are matched to the thickness of the HaP film. This suggests that the MAPI-based solar cell retained its n-i-p character, although, because of photogeneration, the free electron and hole concentrations are orders of magnitude higher than in the dark, and this increases the importance of interface defects. Such a profile implies that the L_D is greater than the film thickness, and in such a case, we cannot determine from EBIC how it changes as a function of illumination, as we only can give a lower estimate of L_D. TRMC measurements done on MAPI films (and not cells) found that the L_D^e has a hill-like feature at $G = 1 \times 10^{22}$ cm^{-3}. Applying the TRMC data to the Rose model plot presented in Figure 6 suggests that the MAPI has $N_r \sim 1 \times 10^{15}$ to 1×10^{14} cm^{-3}.

This relatively low value of recombination states can explain the high performance of iodide-based perovskites, as they possess two essential properties: a n-i-p junction in the cell due to low doping levels and a diffusion length greater than the SC width ($L_D > d_{HaP}$), which limits measurement of L_D to a lower limit.

Our approach is limited only to measurable changes in the L_D under illumination. The sensitivity of the conventional methods for detecting defects can vary between three and 4 orders of magnitude below the carrier population in the bands. The reported density of states (DOS) in the bands near the VBM for different HaP materials is $\sim 1 \times 10^{18}$ cm^{-3}.[49] Here, we estimated the density of recombination centers ~3 orders of magnitude below the DOS in the VBM. Therefore, the new approach presented in this manuscript is considered to have high sensitivity. Another advantage is the ability to measure those materials in their device configuration and reveal an effective density of recombination centers, allowing a comparison between systems. The measured L_D and the calculated parameters results are summarized in Table 1.

CONCLUSIONS

To summarize, we used the in situ EBIC method to visualize the electric field within a working device, assuming that carrier collection is directly related to the electric field.

- The EBIC data indicate no significant recombination or increase in conductivity across the grain boundaries for Ga-FIB-etched cross sections of PV cells.
- The electric field profile line did show a clear difference between a high-performance solar device and a bad one, showing its use as a powerful tool to monitor cell quality.

Table 1. Summary of Electronic Properties and Measurement Conditions for MAPI, $MAPbBr_3(Cl)$, and $MixAPbBr_3$[a]

	MAPI	$MAPbBr_3(Cl)$	$MixAPbBr_3$
doping concentration (cm^{-3})	1×10^{11} to 1×10^{12}	1×10^{12} to 1×10^{14}	1×10^{8} to 1×10^{10}
Illumination intensity [$\mu W/cm^2$]	40–120	1–20	2–120
G (cm^{-3} s^{-1})	1×10^{21} to 1×10^{22}	1×10^{19} to 1×10^{20}	1×10^{20} to 1×10^{21}
L_D EBIC @dark conditions (nm)	>400	50	230
L_D EBIC @illumination conditions (nm)	>400	110	70
L_D from EBIC under illumination	constant	increase	decrease
N_r	1×10^{14} to 1×10^{15}	1×10^{14}	$<1 \times 10^{13}$

[a]Net doping data for MAPI is from ref 49. and the Br-based perovskite are from ref 23.

In addition to those observations, new insights regarding photovoltaic loss mechanisms were found by measuring EBIC with (operando) and without illumination to extract changes in the diffusion/drift length. The changes in the minority carrier diffusion length were modeled by the Rose model. We calculate that polycrystalline films of the mixed A cation $APbBr_3(MixAPbBr_3)$ have a very low electrically active defect concentration (1×10^{13} cm^{-3}) for such films. This approach allows us to evaluate the effective density of those defect states in a solar cell that affects its photovoltaic function.

ASSOCIATED CONTENT

Supporting Information

The Supporting Information is available free of charge at https://pubs.acs.org/doi/10.1021/acsami.1c08675.

EBIC method setup and analysis, sample preparation, and Rose model (PDF)

AUTHOR INFORMATION

Corresponding Authors

David Cahen – *Department of Materials and Interfaces, Weizmann Institute of Science, Rehovot 76100, Israel; Chemistry Department and Institute for Nanotechnology and Advanced Materials, Bar-Ilan University, Ramat Gan 52900, Israel;* orcid.org/0000-0001-8118-5446; Email: david.cahen@weizmann.ac.il

https://doi.org/10.1021/acsami.1c08675
ACS Appl. Mater. Interfaces 2022, 14, 34171–34179

Gary Hodes − *Department of Materials and Interfaces, Weizmann Institute of Science, Rehovot 76100, Israel;* orcid.org/0000-0001-7798-195X; Email: gary.hodes@weizmann.ac.il

Authors

Arava Zohar − *Department of Materials and Interfaces, Weizmann Institute of Science, Rehovot 76100, Israel;* orcid.org/0000-0002-8292-5968

Michael Kulbak − *Department of Materials and Interfaces, Weizmann Institute of Science, Rehovot 76100, Israel*

Silver H. Turren-Cruz − *École Polytechnique Fédérale de Lausanne, Lausanne CH-1015, Switzerland; Institute of Advanced Materials (INAM), Jaume I University, Castelló de la Plana 12071, Spain*

Pabitra K. Nayak − *Department of Physics, Clarendon Laboratory, University of Oxford, Oxford OX1 3PU, United Kingdom; Tata Institute of Fundamental Research, Hyderabad 500046, India;* orcid.org/0000-0002-7845-5318

Adi Kama − *Chemistry Department and Institute for Nanotechnology and Advanced Materials, Bar-Ilan University, Ramat Gan 52900, Israel*

Anders Hagfeldt − *École Polytechnique Fédérale de Lausanne, Lausanne CH-1015, Switzerland;* orcid.org/0000-0001-6725-8856

Henry J Snaith − *Department of Physics, Clarendon Laboratory, University of Oxford, Oxford OX1 3PU, United Kingdom;* orcid.org/0000-0001-8511-790X

Complete contact information is available at: https://pubs.acs.org/10.1021/acsami.1c08675

Notes

The authors declare no competing financial interest.

■ ACKNOWLEDGMENTS

We thank the Yotam project, Ullmann Family Foundation, Dears Foundation, the WIS' Sustainability And Energy Research Initiative, SAERI, and the Minerva Centre for Self-Repairing Systems for Energy & Sustainability for support at the Weizmann Institute and the Israel Ministry of Energy and Infrastructure for the work at Bar-Ilan University. A.Z. thanks Katya Rechav for the FIB sample preparation, Ifat Kaplan-Asheri for assisting with EBIC operation, and Isaac Balberg (Hebrew University of Jerusalem) for fruitful discussions.

■ REFERENCES

(1) Kothandaraman, R. K.; Jiang, Y.; Feurer, T.; Tiwari, A. N.; Fu, F. Near-Infrared-Transparent Perovskite Solar Cells and Perovskite-Based Tandem Photovoltaics. *Small Methods* **2020**, *4* (10), 2000395.

(2) Hu, X.; Jiang, X.-F.; Xing, X.; Nian, L.; Liu, X.; Huang, R.; Wang, K.; Yip, H.-L.; Zhou, G. Wide-Bandgap Perovskite Solar Cells With Large Open-Circuit Voltage of 1653 mV Through Interfacial Engineering. *Sol. RRL* **2018**, *2* (8), 1800083.

(3) Huan, T. N.; Dalla Corte, D. A.; Lamaison, S.; Karapinar, D.; Lutz, L.; Menguy, N.; Foldyna, M.; Turren-Cruz, S.-H.; Hagfeldt, A.; Bella, F.; et al. Low-Cost High-Efficiency System for Solar-Driven Conversion of CO_2 to Hydrocarbons. *Proc. Natl. Acad. Sci. U. S. A.* **2019**, *116* (20), 9735−9740.

(4) Al-Ashouri, A.; Kohnen, E.; Li, B.; Magomedov, A.; Hempel, H.; Caprioglio, P.; Marquez, J. A.; Morales Vilches, A. B.; Kasparavicius, E.; Smith, J. A.; et al. Monolithic Perovskite/Silicon Tandem Solar Cell with > 29% Efficiency by Enhanced Hole Extraction. *Science* **2020**, *370* (6522), 1300−1309.

(5) Egger, D. A.; Bera, A.; Cahen, D.; Hodes, G.; Kirchartz, T.; Kronik, L.; Lovrincic, R.; Rappe, A. M.; Reichman, D. R.; Yaffe, O. What Remains Unexplained about the Properties of Halide Perovskites? *Adv. Mater.* **2018**, *30* (20), 1800691.

(6) Kumar, S.; Hodes, G.; Cahen, D. Defects in Halide Perovskites: The Lattice as a Boojum? *MRS Bull.* **2020**, *45* (6), 478−484.

(7) Ball, J. M.; Petrozza, A. Defects in Perovskite-Halides and Their Effects in Solar Cells. *Nat. Energy* **2016**, *1* (11), 1−13.

(8) Jiang, M.; Wu, Y.; Zhou, Y.; Wang, Z. Observation of Lower Defect Density Brought by Excess PbI_2 in $CH_3NH_3PbI_3$ Solar Cells. *AIP Adv.* **2019**, *9* (8), 085301.

(9) Shi, D.; Adinolfi, V.; Comin, R.; Yuan, M.; Alarousu, E.; Buin, A.; Chen, Y.; Hoogland, S.; Rothenberger, A.; Katsiev, K.; Losovyj, Y.; Zhang, X.; Dowben, P. A.; Mohammed, O. F.; Sargent, E. H.; Bakr, O. M. Low Trap-State Density and Long Carrier Diffusion in Organolead Trihalide Perovskite Single Crystals. *Science* **2015**, *347* (6221), 519−522.

(10) Brenner, T. M.; Egger, D. A.; Kronik, L.; Hodes, G.; Cahen, D. Hybrid Organic—Inorganic Perovskites: Low-Cost Semiconductors with Intriguing Charge-Transport Properties. *Nat. Rev. Mater.* **2016**, *1* (1), 1−16.

(11) Sherkar, T. S.; Momblona, C.; Gil-Escrig, L.; Bolink, H. J.; Koster, L. J. A. Improving Perovskite Solar Cells: Insights From a Validated Device Model. *Adv. Energy Mater.* **2017**, *7* (13), 1602432.

(12) Abou-Ras, D.; Kirchartz, T. Electron-Beam-Induced Current Measurements of Thin-Film Solar Cells. *ACS Appl. Energy Mater.* **2019**, *2* (9), 6127−6139.

(13) Reuter, P.; Rath, T.; Fischereder, A.; Trimmel, G.; Hadley, P. Electron Beam-Induced Current (EBIC) in Solution-Processed Solar Cells. *Scanning* **2011**, *33* (1), 1−6.

(14) Cahen, D.; Noufi, R. Defect Chemical Explanation for the Effect of Air Anneal on CdS/$CuInSe_2$ Solar Cell Performance. *Appl. Phys. Lett.* **1989**, *54* (6), 558−560.

(15) Kedem, N.; Brenner, T. M.; Kulbak, M.; Schaefer, N.; Levcenko, S.; Levine, I.; Abou-Ras, D.; Hodes, G.; Cahen, D. Light-Induced Increase of Electron Diffusion Length in a p−n Junction Type $CH_3NH_3PbBr_3$ Perovskite Solar Cell. *J. Phys. Chem. Lett.* **2015**, *6* (13), 2469−2476.

(16) Klein-Kedem, N.; Cahen, D.; Hodes, G. Effects of Light and Electron Beam Irradiation on Halide Perovskites and Their Solar Cells. *Acc. Chem. Res.* **2016**, *49* (2), 347−354.

(17) Edri, E.; Kirmayer, S.; Mukhopadhyay, S.; Gartsman, K.; Hodes, G.; Cahen, D. Elucidating the Charge Carrier Separation and Working Mechanism of $CH_3NH_3PbI_{3-x}Cl_x$ Perovskite Solar Cells. *Nat. Commun.* **2014**, *5*, 3461.

(18) Park, B.; Kedem, N.; Kulbak, M.; Lee, D. Y.; Yang, W. S.; Jeon, N. J.; Seo, J.; Kim, G.; Kim, K. J.; Shin, T. J.; Hodes, G.; Cahen, D.; Seok, S. I. Understanding How Excess Lead Iodide Precursor Improves Halide Perovskite Solar Cell Performance. *Nat. Commun.* **2018**, *9* (1), 3301.

(19) Kedem, N.; Kulbak, M.; Brenner, T. M.; Hodes, G.; Cahen, D. Type-Inversion as a Working Mechanism of High Voltage $MAPbBr_3$(Cl)-Based Halide Perovskite Solar Cells. *Phys. Chem. Chem. Phys.* **2017**, *19* (8), 5753−5762.

(20) Philippe, B.; Saliba, M.; Correa-Baena, J.-P.; Cappel, U. B.; Turren-Cruz, S.-H.; Grätzel, M.; Hagfeldt, A.; Rensmo, H. Chemical Distribution of Multiple Cation (Rb + , Cs + , MA + , and FA +) Perovskite Materials by Photoelectron Spectroscopy. *Chem. Mater.* **2017**, *29* (8), 3589−3596.

(21) Kulbak, M.; Levine, I.; Barak-Kulbak, E.; Gupta, S.; Zohar, A.; Balberg, I.; Hodes, G.; Cahen, D. Control over Self-Doping in High Band Gap Perovskite Films. *Adv. Energy Mater.* **2018**, *8* (23), 1800398.

(22) McMeekin, D. P.; Sadoughi, G.; Rehman, W.; Eperon, G. E.; Saliba, M.; Hörantner, M. T.; Haghighirad, A.; Sakai, N.; Korte, L.; Rech, B.; Johnston, M. B.; Herz, L. M.; Snaith, H. J. A Mixed-Cation Lead Mixed-Halide Perovskite Absorber for Tandem Solar Cells. *Science* **2016**, *351* (6269), 151−155.

(23) Levine, I.; Gupta, S.; Bera, A.; Ceratti, D.; Hodes, G.; Cahen, D.; Guo, D.; Savenije, T. J.; Ávila, J.; Bolink, H. J.; Millo, O.; Azulay, D.; Balberg, I. Can We Use Time-Resolved Measurements to Get Steady-

State Transport Data for Halide Perovskites? *J. Appl. Phys.* **2018**, *124* (10), 103103.
(24) Edri, E.; Kirmayer, S.; Henning, A.; Mukhopadhyay, S.; Gartsman, K.; Rosenwaks, Y.; Hodes, G.; Cahen, D. Why Lead Methylammonium Tri-Iodide Perovskite-Based Solar Cells Require a Mesoporous Electron Transporting Scaffold (but Not Necessarily a Hole Conductor). *Nano Lett.* **2014**, *14* (2), 1000−1004.
(25) Adhyaksa, G. W. P.; Brittman, S.; Āboliņš, H.; Lof, A.; Li, X.; Keelor, J. D.; Luo, Y.; Duevski, T.; Heeren, R. M. A.; Ellis, S. R.; Fenning, D. P.; Garnett, E. C. Understanding Detrimental and Beneficial Grain Boundary Effects in Halide Perovskites. *Adv. Mater.* **2018**, *30* (52), 1804792.
(26) Yin, W.-J.; Shi, T.; Yan, Y. Unique Properties of Halide Perovskites as Possible Origins of the Superior Solar Cell Performance. *Adv. Mater.* **2014**, *26* (27), 4653−4658.
(27) Cohen, A. V.; Egger, D. A.; Rappe, A. M.; Kronik, L. Breakdown of the Static Picture of Defect Energetics in Halide Perovskites: The Case of the Br Vacancy in $CsPbBr_3$. *J. Phys. Chem. Lett.* **2019**, *10* (16), 4490−4498.
(28) Sherkar, T. S.; Momblona, C.; Gil-Escrig, L.; Ávila, J.; Sessolo, M.; Bolink, H. J.; Koster, L. J. A. Recombination in Perovskite Solar Cells: Significance of Grain Boundaries, Interface Traps, and Defect Ions. *ACS Energy Lett.* **2017**, *2* (5), 1214−1222.
(29) Yun, J. S.; Ho-Baillie, A.; Huang, S.; Woo, S. H.; Heo, Y.; Seidel, J.; Huang, F.; Cheng, Y.-B.; Green, M. A. Benefit of Grain Boundaries in Organic−Inorganic Halide Planar Perovskite Solar Cells. *J. Phys. Chem. Lett.* **2015**, *6* (5), 875−880.
(30) Visoly-Fisher, I.; Cohen, S. R.; Ruzin, A.; Cahen, D. How Polycrystalline Devices Can Outperform Single-Crystal Ones: Thin Film CdTe/CdS Solar Cells. *Adv. Mater.* **2004**, *16* (11), 879−883.
(31) Azulay, D.; Millo, O.; Balberg, I.; Schock, H.-W.; Visoly-Fisher, I.; Cahen, D. Current Routes in Polycrystalline $CuInSe_2$ and Cu(In, Ga)Se_2 Films. *Sol. Energy Mater. Sol. Cells* **2007**, *91* (1), 85−90.
(32) Gordillo, G.; Otálora, C. A.; Reinoso, M. A. Trap Center Study in Hybrid Organic-Inorganic Perovskite Using Thermally Stimulated Current (TSC) Analysis. *J. Appl. Phys.* **2017**, *122* (7), 075304.
(33) Qin, C.; Matsushima, T.; Fujihara, T.; Potscavage, W. J.; Adachi, C. Degradation Mechanisms of Solution-Processed Planar Perovskite Solar Cells: Thermally Stimulated Current Measurement for Analysis of Carrier Traps. *Adv. Mater.* **2016**, *28* (3), 466−471.
(34) Baumann, A.; Väth, S.; Rieder, P.; Heiber, M. C.; Tvingstedt, K.; Dyakonov, V. Identification of Trap States in Perovskite Solar Cells. *J. Phys. Chem. Lett.* **2015**, *6* (12), 2350−2354.
(35) Heo, S.; Seo, G.; Lee, Y.; Lee, D.; Seol, M.; Lee, J.; Park, J.-B.; Kim, K.; Yun, D.-J.; Kim, Y. S.; Shin, J. K.; Ahn, T. K.; Nazeeruddin, M. K. Deep Level Trapped Defect Analysis in $CH_3NH_3PbI_3$ Perovskite Solar Cells by Deep Level Transient Spectroscopy. *Energy Environ. Sci.* **2017**, *10* (5), 1128−1133.
(36) Rosenberg, J. W.; Legodi, M. J.; Rakita, Y.; Cahen, D.; Diale, M. Laplace Current Deep Level Transient Spectroscopy Measurements of Defect States in Methylammonium Lead Bromide Single Crystals. *J. Appl. Phys.* **2017**, *122* (14), 145701.
(37) Eames, C.; Frost, J. M.; Barnes, P. R. F.; O'Regan, B. C.; Walsh, A.; Islam, M. S. Ionic Transport in Hybrid Lead Iodide Perovskite Solar Cells. *Nat. Commun.* **2015**, *6*, 7497.
(38) Bag, M.; Renna, L. A.; Adhikari, R. Y.; Karak, S.; Liu, F.; Lahti, P. M.; Russell, T. P.; Tuominen, M. T.; Venkataraman, D. Kinetics of Ion Transport in Perovskite Active Layers and Its Implications for Active Layer Stability. *J. Am. Chem. Soc.* **2015**, *137* (40), 13130−13137.
(39) Yuan, Y.; Huang, J. Ion Migration in Organometal Trihalide Perovskite and Its Impact on Photovoltaic Efficiency and Stability. *Acc. Chem. Res.* **2016**, *49* (2), 286−293.
(40) Futscher, M. H.; Lee, J. M.; McGovern, L.; Muscarella, L. A.; Wang, T.; Haider, M. I.; Fakharuddin, A.; Schmidt-Mende, L.; Ehrler, B. Quantification of Ion Migration in $CH_3NH_3PbI_3$ Perovskite Solar Cells by Transient Capacitance Measurements. *Mater. Horiz.* **2019**, *6* (7), 1497−1503.
(41) Yang, T.-Y.; Gregori, G.; Pellet, N.; Grätzel, M.; Maier, J. The Significance of Ion Conduction in a Hybrid Organic−Inorganic Lead-Iodide-Based Perovskite Photosensitizer. *Angew. Chem., Int. Ed.* **2015**, *54* (27), 7905−7910.
(42) Lee, H.; Gaiaschi, S.; Chapon, P.; Tondelier, D.; Bourée, J.-E.; Bonnassieux, Y.; Derycke, V.; Geffroy, B. Effect of Halide Ion Migration on the Electrical Properties of Methylammonium Lead Tri-Iodide Perovskite Solar Cells. *J. Phys. Chem. C* **2019**, *123* (29), 17728−17734.
(43) Peng, W.; Aranda, C.; Bakr, O. M.; Garcia-Belmonte, G.; Bisquert, J.; Guerrero, A. Quantification of Ionic Diffusion in Lead Halide Perovskite Single Crystals. *ACS Energy Lett.* **2018**, *3* (7), 1477−1481.
(44) Birkhold, S. T.; Precht, J. T.; Giridharagopal, R.; Eperon, G. E.; Schmidt-Mende, L.; Ginger, D. S. Direct Observation and Quantitative Analysis of Mobile Frenkel Defects in Metal Halide Perovskites Using Scanning Kelvin Probe Microscopy. *J. Phys. Chem. C* **2018**, *122* (24), 12633−12639.
(45) Almora, O.; Guerrero, A.; Garcia-Belmonte, G. Ionic Charging by Local Imbalance at Interfaces in Hybrid Lead Halide Perovskites. *Appl. Phys. Lett.* **2016**, *108* (4), 043903.
(46) San, G.; Balberg, M.; Jedrzejewski, J.; Balberg, I. The Phototransport in Halide Perovskites: From Basic Physics to Applications. *J. Appl. Phys.* **2020**, *127* (8), 085103.
(47) Motta, C.; El-Mellouhi, F.; Sanvito, S. Charge Carrier Mobility in Hybrid Halide Perovskites. *Sci. Rep.* **2015**, *5* (1), 12746.
(48) Levine, I.; Gupta, S.; Brenner, T. M.; Azulay, D.; Millo, O.; Hodes, G.; Cahen, D.; Balberg, I. Mobility−Lifetime Products in $MAPbI_3$ Films. *J. Phys. Chem. Lett.* **2016**, *7* (24), 5219−5226.
(49) Leijtens, T.; Eperon, G. E.; Barker, A. J.; Grancini, G.; Zhang, W.; Ball, J. M.; Kandada, A. R. S.; Snaith, H. J.; Petrozza, A. Carrier Trapping and Recombination: The Role of Defect Physics in Enhancing the Open Circuit Voltage of Metal Halide Perovskite Solar Cells. *Energy Environ. Sci.* **2016**, *9* (11), 3472−3481.

https://doi.org/10.1021/acsami.1c08675
ACS Appl. Mater. Interfaces 2022, 14, 34171−34179